HOKKAIDO UNIVERSITY

Title	Assembly of electric double-layer capacitors with hardwood kraft lignin-based electrodes and separator together with ionic liquid electrolyte
Author(s)	Pakkang, Nutthira; Suzuki, Shiori; Shigetomi, Kengo et al.
Citation	Holzforschung, 77(2), 119-126 https://doi.org/10.1515/hf-2022-0143
Issue Date	2022-12-15
Doc URL	https://hdl.handle.net/2115/90926
Type	journal article
File Information	10.1515_hf-2022-0143.pdf

Original Article

Nutthira Pakkang, Shiori Suzuki, Kengo Shigetomi and Yasumitsu Uraki*

Assembly of electric double-layer capacitors with hardwood kraft lignin-based electrodes and separator together with ionic liquid electrolyte

Abstract: This study aimed to assemble a high-performance electric double-layer capacitor (EDLC) using a hardwood kraft lignin (HKL)-based separator and HKL-based electrodes, which were fabricated from a nonwoven mat of electrospun HKL fibers. The separator was prepared by the thermostabilization of the mat derived from a mixed dope of HKL, hexamethylenetetramine, and polyethylene glycol (1.66/0.50/0.09, w/w) for electrospinning. Although a mat-type HKL-based electrode containing conductive carbon black (CB) has been reported to be suitable for a commercial cellulosic separator, this electrode was found to be unsuitable for the HKL-based separator because of its rough surface and poor contact with the separator interface. Hence, a powder-type electrode with a smooth surface was fabricated by grinding the mat, followed by casting with a carboxymethyl cellulose aqueous solution, and its EDLC possessed high energy (49 Wh kg^{-1}) and power densities (151 kW kg^{-1}). Moreover, to provide a simple process for electrode fabrication, another mat-type electrode was fabricated by adding CB to the mixed dope, followed by electrospinning, carbonization, and steam activation. The resultant EDLC exhibited excellent electrochemical performance with energy (58 Wh kg^{-1}) and power densities (55 kW kg^{-1}).

Keywords: electric double layer capacitor; electrode; kraft lignin; separator; supercapacitor.

*Corresponding author: Yasumitsu Uraki, Research Faculty of Agriculture, Hokkaido University, Sapporo 060-8589, Japan,
E-mail: uraki@for.agr.hokudai.ac.jp
Nutthira Pakkang, Graduate School of Agriculture, Hokkaido University, Sapporo 060-8589, Japan
Shiori Suzuki and Kengo Shigetomi, Research Faculty of Agriculture, Hokkaido University, Sapporo 060-8589, Japan. https://orcid.org/0000-0001-9560-8091 (K. Shigetomi)

1 Introduction

Electric double-layer capacitors (EDLCs) with high performance, termed as supercapacitors, are promising electrical energy storage devices. They provide high power density besides the advantage of quick charging/discharging time and longer cyclability than lithium-ion batteries (LIBs) (Fthenakis and Nikolakakis 2012; Miller and Butler 2021; Najib and Erdem 2019). An EDLC comprises three main parts: a separator, a pair of electrodes, and an electrolyte. Generally, the separator and the electrode are produced from petroleum-derived materials (Funabashi 2016; Pai et al. 2021; Wang et al. 2021). To replace them with renewable resource-based materials, studies on the development of EDLC parts from biomass feedstock have been promoted, especially from woody biomass such as cellulose and lignin (Jiang et al. 2017; Köse et al. 2018; Li et al. 2019; Nguyen et al. 2020; Taer et al. 2021; Takeuchi et al. 2018).

There are several reports on the preparation of EDLC electrodes from technical lignin (Du et al. 2021; Saha et al. 2014; Suzanowicz et al. 2022; Zhu et al. 2020). Among these electrodes, a mat-type electrode, prepared from a mixed dope of kraft lignin, hexamethylene tetramine, and polyethylene glycol by electrospinning with spraying a suspension of conductive carbon black (CB), was suitable for a commercial cellulosic separator, resulting in an EDLC with high energy and power densities (Pakkang et al. 2020). However, there are only a few reports on lignin-based EDLC separators (Koda et al. 2019; Park et al. 2019; Taira et al. 2019). Particularly, kraft lignin has never been employed for designing an EDLC separator, despite being produced in large quantities as a byproduct of kraft pulping. Moreover, there is no report on the assembly of EDLCs using a lignin-based electrode and separator. Hence, this study aims to develop hardwood kraft lignin (HKL)-based EDLCs with high performance by fabricating and combining HKL-based electrodes and separator.

In this study, a nonwoven mat was fabricated by electrospinning of HKL and thereafter converted to an EDLC separator, according to a previous report on lignin-based LIB separators (Uddin et al. 2017; Zhao et al. 2015). This

nonwoven mat was further converted to an EDLC electrode with a large surface area by carbonization and subsequent steam activation (García-Mateos et al. 2020; Hu et al. 2014; Wu et al. 2021). Thus, the advantage of these preparation methods is that both the separator and electrode for EDLCs can be simply fabricated from the same starting material (i.e., a nonwoven mat).

EDLCs have the drawback of a low energy density compared with LIBs. The energy density (E) is expressed by the following equation:

$$E = 1/8CV^2, \tag{1}$$

where C is the electrostatic capacitance and V is the voltage window (Kim et al. 2013). Therefore, either C or V should be enhanced to improve the energy density. Hence, in this study, an ionic liquid (IL) is used as an electrolyte to enhance V. This follows from the fact that ILs can be operated at a wider voltage window (ca. 3.5 V) (Yan et al. 2018) than other electrolytes, such as aqueous (ca. 1.0 V) (Lai et al. 2021) and organic electrolytes (ca. 3.0 V) (Nguyen et al. 2021). Consequently, this study demonstrates EDLCs with high energy and power densities, assembled using HKL-based electrodes and an HKL-based separator together with an IL electrolyte.

2 Materials and methods

2.1 Materials

All chemicals used in this study were obtained as previously reported (Pakkang et al. 2020). Briefly, hardwood kraft lignin (HKL) was prepared from a black liquor of kraft pulping (Nippon Paper Industries Co., Ltd.) by acidification, filtration, and lyophilization. Polyethylene glycol (PEG, 500 kDa), hexamethylenetetramine (Hex), activated carbon (AC) powder, and other chemicals were purchased from FUJIFILM Wako Pure Chemical Industries, Co., Ltd. Moreover, 1-ethyl-3-methylimidazolium tetrafluoroborate (EmimBF$_4$, >97.0%), used as an IL electrolyte, was purchased from Tokyo Chemical Industry Co., Ltd.

2.2 Preparation of HKL-based separator (tHKL separator)

A preparation scheme of an EDLC separator and electrodes is shown in Figure 1. HKL (1.66 g) was mixed with PEG (0.09 g) in a binary solvent of N,N-dimethylformamide (DMF, 1.65 g) and acetic acid (AcOH, 1.10 g). The mixture was stirred at 80 °C for 1 h to obtain a homogeneous solution. Hex (0.50 g) was then added to the solution with stirring at 80 °C for 2 h. The resultant solution was electrospun under the same condition as previously reported (Pakkang et al. 2020). Briefly, the employed parameters were as follows: applied voltage = 18 kV, needle tip–collector distance = 13 cm, and solution flow rate = 2 mL h^{-1}. The electrospun fiber mat was thermostabilized by heating in the air from room temperature (RT, 25 °C) to 250 °C at a heating rate of 2 °C min^{-1}. After reaching 250 °C, the temperature was maintained for 1 h and then decreased to RT to
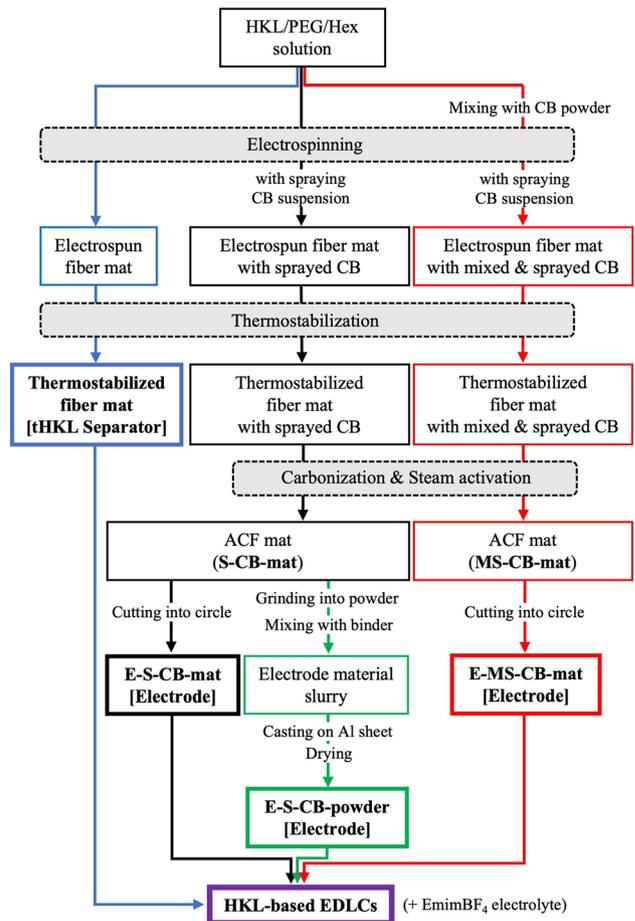

Figure 1: Preparation of a hardwood kraft lignin (HKL)-based separator, HKL-based mat/powder-type electrodes, and the assembled electrical double-layer capacitors (EDLCs) with EmimBF$_4$ as an ionic liquid (IL) electrolyte.

obtain a thermostabilized fiber mat. The mat was cut into a circular shape of 18 mm diameter, denoted as a "tHKL separator".

2.3 Preparation of HKL-based electrodes

2.3.1 Mat-type electrode via spraying CB (E-S-CB-mat): The dope of HKL/PEG/Hex in DMF/AcOH was electrospun by the same procedure as described in Section 2.2. After 15 min of electrospinning, 1 wt% conductive carbon black (CB) suspension in acetone was sprayed onto the electrospun fiber mat several times until electrospinning was completed (see Supplementary Figure S1 for the detail procedure). The resultant mass of CB in the mat was 5 wt% based on the electrospun fibers. Furthermore, the mat was thermostabilized under the same condition as described in Section 2.2. The thermostabilized fiber mat was subsequently carbonized by heating from RT to 900 °C at a heating rate of 3 °C min^{-1}. Thereafter, the temperature was maintained for 1 h under N$_2$ flow (0.5 L min^{-1}). Finally, steam was introduced into the furnace at 900 °C together with N$_2$ flow (You et al. 2016). The resultant activated carbon fiber (ACF) mat was denoted as an "S-CB-mat". This mat was cut into a circular shape of 16 mm diameter and directly used as a mat-type electrode, denoted as an "E-S-CB-mat".

2.3.2 Powder-type electrode via griding and casting (E-S-CB-powder): S-CB-mat, prepared in Section 2.3.1, was ground into a fine powder using a pestle and mortar. The ACF powder was then mixed with a 2% aqueous solution of carboxymethyl cellulose (CMC) as a binder at an ACF/CMC ratio of 9/1 (w/w). The resultant slurry was cast on an aluminum sheet using a doctor blade and dried overnight in an oven at 105 ℃. The coated aluminum sheet was cut into a circular shape of 16 mm diameter. This powder-type electrode was denoted as an "E-S-CB-powder".

As a reference of the powder-type electrode, a commercial AC powder and CB (85/5, w/w) were mixed and cast on an aluminum sheet together with the 2% CMC aqueous solution according to a previously reported procedure (You et al. 2015). The coated aluminum sheet was cut into a circular shape of 16 mm diameter. This powder-type electrode was denoted as an "E-AC powder".

2.3.3 Another mat-type electrode via mixing and spraying CB (E-MS-CB-mat): The dope of HKL/PEG/Hex in DMF/AcOH was prepared by the same procedure as described in Section 2.2. CB fine powder (0.025 g, 0.5 wt % on HKL) was added to the dope with stirring for 30 min at RT. The mixture was electrospun under the same conditions as described in Section 2.2. During the electrospinning, a 1 wt% CB suspension in acetone was sprayed onto the mat several times. The splaying process was continued until 1 min earlier to the completion of electrospinning. The resultant CB mass was 4.5 wt%. Furthermore, the mat was thermo-stabilized, carbonized, and steam-activated under the same conditions as described in Section 2.3.1. The resultant ACF mat was denoted as "MS-CB-mat". This mat was cut into a circular shape of 16 mm diameter and directly used as a mat-type electrode, denoted as an "E-MS-CB-mat".

2.4 EDLC assembly

All EDLCs were assembled in a dry glove box filled with N_2 gas.

2.4.1 EDLCs with mat-type electrodes: An aluminum sheet, a mat-type electrode (E-S-CB-mat or E-MS-CB-mat), and a tHKL separator were successively placed at the bottom of an EDLC measurement cell (2E-CELL-SUS, Eager Co., Ltd.). Several droplets of $EmimBF_4$, used as an IL electrolyte, were placed on the separator. Then, another mat-type electrode and an aluminum sheet were placed on the separator, consecutively.

2.4.2 EDLCs with powder-type electrodes: The powder-type electrode (E-S-CB-powder) was soaked in $EmimBF_4$ *in vacuo* for 2 h. After removing the excess electrolyte using Kimwipe, the side of the aluminum sheet in the soaked electrode was placed on the bottom of the measurement cell, and the tHKL separator was layered on top. Finally, the ACF side of the other soaked electrode was placed on the separator.

The reference electrode (E-AC powder) was assembled with a commercial cellulosic separator to prepare a reference EDLC.

2.5 Instrumental analyses

The morphology of the electrodes was observed using three-dimensional (3D) laser microscopes (VK-9500 and VHX-970F, Keyence Japan, Co., Ltd.). The arithmetical mean height in line (R_a) was obtained from the line scan in the captured image range of 50 μm × 75 μm using VHX-970F with an objective lens of ×2000 magnification. The extension of R_a in the four measurements (100 μm × 150 μm) is the arithmetical mean height (S_a) as a surface roughness according to ISO 25178 (see supporting information for the two-dimensional (2D) and 3D images in Supplementary Figure S2 and the calculation details for R_a and S_a).

The electrical surface resistance of the mat-type electrodes was examined using a low-resistivity meter (Loresta-AX-MCP-T370, Mitsubishi Chemical Analytech Co., Ltd.). Resistivity was measured by pushing the probe with the linear 4-pin onto the mat surface (2 cm × 2 cm) at five different positions, and the average resistance was calculated.

Prior to the measurement of N_2 adsorption–desorption, all ACF mats were ground into powders using a mortar and pestle, according to ISO 9277:2010. The measurement was conducted by a surface area analyzer (Autosorb-1, Quantachrome Instruments Japan Co. Ltd.) at –196 ℃. The specific surface area was calculated from the adsorption isotherm ranging from the relative pressure (P/P_0) range of 0.02–0.30 using the Brunauer–Emmett–Teller (BET) model. The internal and external surface areas were estimated from the *t*-plot method in the P/P_0 range of 0.2–0.5 (You et al. 2015). The average pore size and distribution were calculated from the adsorption isotherms according to the quenched solid density functional theory (QSDFT) (Neimark et al. 2009).

The electrochemical performance of EDLCs was evaluated using an electrochemical workstation (Autolab PGSTAT302N FRA32M, Metrohm Autolab B.V.). The specific capacitance of EDLCs in the potential window of 0–3.5 V was calculated from the area of cyclic voltammogram (CV) and discharge slope of galvanostatic charge-discharge (GCD) profiles, according to previous reports (Kim et al. 2013; You et al. 2015).

Electrochemical impedance spectroscopy (EIS) was conducted to measure the impedance between 100 kHz and 1 Hz at an AC amplitude of 10 mV. The charge transfer resistance (R_{ct}) and the intrinsic resistance (R_i) were calculated from the diameter of the semicircle and intercept on the Z′ axis of the Nyquist plots, respectively (Mei et al. 2017).

The energy density (E) was estimated based on the Eq. (1) as described in the Introduction section. In Eq. (1), C (F g^{-1}) is the specific capacitance calculated from the GCD measurement and V is the voltage window (3.5 V).

The power density (P) was estimated from the following equation:

$$P = i(V - V_{drop})^2 / 2mV_{drop}, \tag{2}$$

where i (A) is a constant current, m (g) is the total weight of the electrode on the aluminum sheet, and V_{drop} (V) is the voltage drop obtained from the gap between 3.5 V and the beginning of the discharge (Kim et al. 2013).

3 Results and discussion

3.1 Preparation of HKL-based separator (tHKL separator)

Generally, EDLC separators are required to have porosity, dimensional stability, and resistance to chemicals, especially to electrolytes (Xian-Zhong et al. 2014). A nonwoven mat of electrospun HKL fibers can be a promising candidate, but the mat was partly soluble in some organic solvents and ILs. Therefore, the mat was converted into an insoluble mat by following a procedure. Firstly, the HKL/
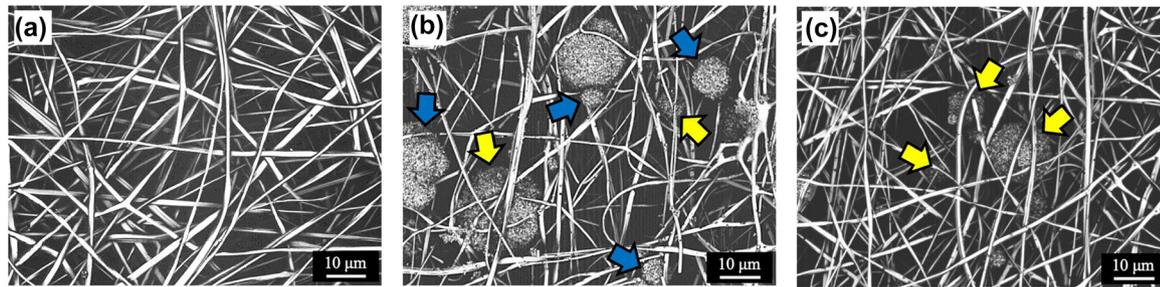
Figure 2: Microscopic images of (a) tHKL separator, (b) E-S-CB-mat, and (c) E-MS-CB-mat. Blue arrows indicate the CB aggregates located on the mat surface. Yellow arrows indicate the CB aggregates located inside the mat.

PEG/Hex dope was electrospun with the aid of PEG (Pakkang et al. 2020; Zakaria et al. 2021). Subsequently, the electrospun fiber mat was efficiently thermostabilized at a rapid heating rate of 2 °C min^{-1} owing to the assistance of Hex as a crosslinker (Lin et al. 2013; Martin et al. 2006). Consequently, the thermostabilized HKL-based mat became insoluble in the IL electrolyte, EmimBF$_4$. This was owing to the generation of a network structure between HKL molecules. The microscopic image of the HKL-based thermostabilized fiber mat (Figure 2a) indicates that each fiber had a smooth surface with a surface roughness (S_a) of 1.81 ± 0.27 μm and an average fiber diameter of 0.94 ± 0.32 μm. This mat was used as an EDLC separator (tHKL separator) and assembled with the electrodes and EmimBF$_4$ electrolyte to fabricate the EDLCs.

3.2 Preparation of mat-type electrode (E-S-CB-mat) and its EDLC

A mat-type electrode containing 5 wt% CB (E-S-CB-mat) was previously reported (Pakkang et al. 2020). The EDLC assembled with a commercial cellulosic separator exhibited high energy density (91.5 Wh kg^{-1}) and power density (76.2 kW kg^{-1}). However, as shown in Table 1, the EDLC assembled with E-S-CB-mat and tHKL separator showed relatively low power density, although it exhibited comparatively high energy density and high specific capacitance, as

estimated by using CV (Figure S3) and GCD measurements. The lower power density was attributed to the large V_{drop} at the changing point from the charging to discharging process in the GCD measurement as shown in Figure 3a, b. The V_{drop} reflects the efficiency of electrolyte ions being desorbed from electrodes. The desorption efficiency depends on the surface resistance of electrodes and the distance between the electrode and separator. Therefore, lower resistance and shorter distance (i.e., better contact) contribute to higher efficiency, expressed as a smaller V_{drop} (Hamsan et al. 2020; Nguyen and Breitkopf 2018). Although both the R_{ct} and R_i resistances of E-S-CB-mat were sufficiently low (Table 1 and Figure S4), it showed the large V_{drop} (Figure 3b). This could be due to the large surface roughness of the E-S-CB-mat, resulting in poor contact with the separator interface and high surface resistance (Table 2). Hence, the development of an improved electrode with smooth surfaces was subsequently attempted.

3.3 Preparation of powder-type electrode (E-S-CB-powder) and its EDLC

A casting technique of electrode materials on a current collector (typically, an aluminum sheet) is widely used, because this technique can provide flat surfaces of the electrode, resulting in its good contact with a separator (Chakrabarti

Table 1: Electrochemical performance of the assembled EDLCs at a voltage window of 0–3.5 V.

Electrode	Separator	C_{sp}[a] (GCD) (F g^{-1})	C_{sp}[b] (CV) (F g^{-1})	R_{ct}[c] (Ohm)	R_i[d] (Ohm)	Energy density (Wh kg^{-1})	Power density (Wh kg^{-1})
E-S-CB-mat[e]	tHKL	127.4	100.3	0.32	1.41	54.2	26.3
E-S-CB-powder	tHKL	114.3	90.7	1.20	1.90	48.6	151.0
E-MS-CB-mat	tHKL	136.1	110.8	1.63	3.19	57.9	55.0
E-AC-powder	Cellulosic	97.5	88.4	1.51	3.45	41.5	93.1

[a]Calculated by GCD method; [b]calculated by CV method; [c]charge transfer resistance; [d]intrinsic resistance. [e]This E-S-CB-mat corresponds to "ACF-95/5-5CB" in our previous article (Pakkang et al. 2020).
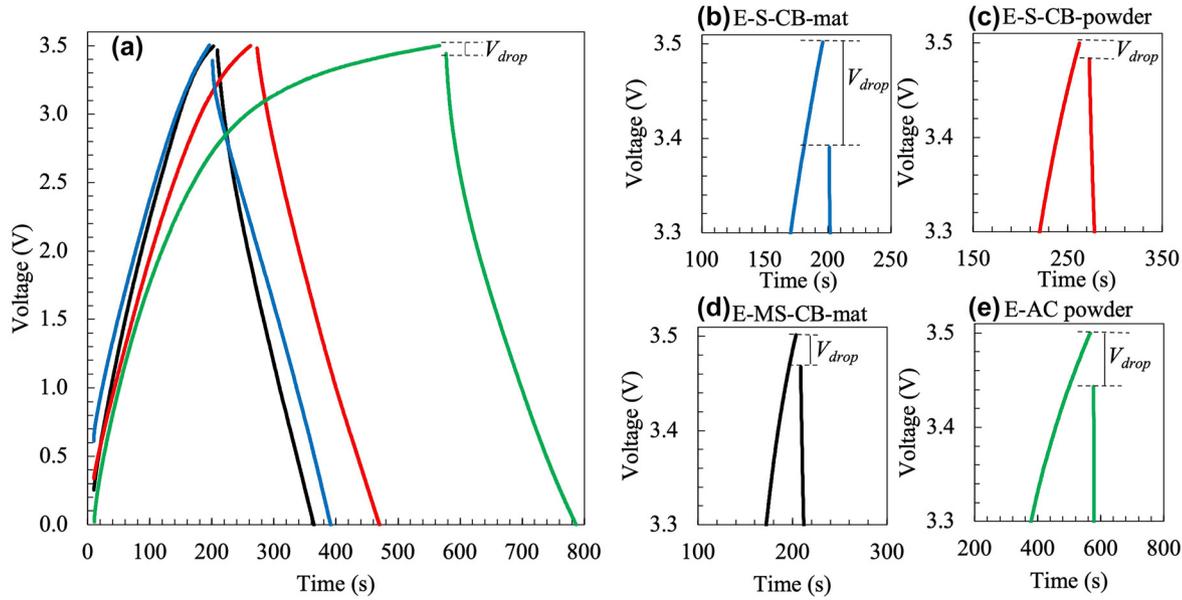

Figure 3: GCD profiles of (a) four types of EDLCs assembled in this study at a current density of 1 A g^{-1}. Magnified GCD profiles of (b) E-S-CB-mat, (c) E-S-CB-powder, (d) E-MS-CB-mat, and (e) E-AC powder for V_{drop} regions as shown between 3.3 and 3.5 V.

Table 2: Surface roughness and electric resistance of the electrodes.

Electrode	Surface roughness (μm)	Surface resistance (Ω)
E-S-CB-mat	3.67 ± 0.72	95.4 ± 11.7
E-S-CB-powder	1.96 ± 0.17	1.56 ± 0.66
E-MS-CB-mat	2.31 ± 0.38	19.5 ± 4.73
E-AC-powder	1.13 ± 0.94	0.20 ± 0.07

and Low 2021; He et al. 2017; Kasprzak et al. 2018). Accordingly, S-CB-mat was ground into a powder, blended with CMC as a binder, and then cast on an aluminum sheet to prepare a powder-type electrode (E-S-CB-powder). As expected, E-S-CB-powder exhibited the smallest surface roughness (1.96 ± 0.17 μm) among all HKL-based electrodes prepared in this study (Table 2). The surface resistance (1.56 ± 0.66 Ω) was also the lowest. Consequently, the V_{drop} of its EDLC assembled with tHKL separator (Figure 3c) drastically decreased to approximately 1/5 of that for E-S-CB-mat, leading to the highest power density (151 kW kg^{-1}) among all EDLCs prepared in this study (Table 1).

3.4 Preparation of another mat-type electrode (E-MS-CB-mat) and its EDLC

E-S-CB-powder, described in Section 3.3, resulted in an excellent HKL-based EDLC, but the preparation for the powder-type electrode is arduous. Therefore, another

improved mat-type electrode, that can be employed in conjunction with the tHKL separator, was developed. The large surface roughness of the previous mat-type electrode (E-S-CB-mat) was attributed to the exposure of CB aggregates with diameters of 5–20 μm to the mat surface (Figure 2b). These aggregates were formed from fine CB powders with an average diameter of 0.042 μm when spraying an acetone-CB suspension on the mat during electrospinning. Hence, to suppress the exposure of CB aggregates, the electrospinning of the HKL-containing dope was extended to 1 min after the end of the spraying of the CB suspension. The resultant mat was subsequently converted into an ACF mat by carbonization and steam activation. Consequently, the surface roughness of this mat improved to 1.81 ± 0.27 μm, but the surface resistance (606 ± 66 Ω) was much higher than that of E-S-CB-mat (Table 2), suggesting that the conductivity of the mat surface was not enhanced by distribution of the CB aggregates inside the mat.

To reduce the surface resistance of this ACF mat, CB fine powders were directly mixed into the HKL-containing dope, where the CB content was 0.5 wt.% on HKL. The CB-mixed dope was electrospun with a spraying of the CB suspension, and the electrospinning was conducted until 1 min after the end of spraying. The resultant mat was then converted into an ACF mat in the same manner as mentioned previously. As shown in Figure 2c, CB aggregates were not exposed to the surface of E-MS-CB-mat and covered by ACFs. Consequently, its surface roughness and resistance remarkably decreased to 63% and 20% of those

Table 3: Surface area and pore distribution of ACF mats and reference materials.

Sample	Specific surface area[a] BSA (m^2 g^{-1})	Total pore volume (cm^3 g^{-1})	Average pore diameter[b] Micropore	Mesopore	Ratio of internal/external surface areas[c]
S-CB-mat	1090	0.56	0.80 (93%)	3.23 (7%)	4.04 (817/202)
MS-CB-mat	765	0.52	0.96 (83%)	3.58 (17%)	1.68 (480/285)
CB powder	63	0.06	1.12 (47%)	3.18 (53%)	0.02 (1/16)
Activated-CB powder	96	0.08	1.04 (63%)	3.12 (37%)	0.19 (15/81)
AC powder	1670	1.26	1.15 (67%)	3.23 (33%)	0.18 (259/1412)

[a]Calculated by the BET model; [b]calculated based on the QSDFT model and the parentheses is a percentage volume ratio; [c]calculated according to the *t*-plot model and the unit of parentheses value is m^2 g^{-1}.

of E-S-CB-mat, respectively (Table 2). However, the BET surface area of MS-CB-mat was smaller than that of S-CB-mat, although the average mesopore diameter and volume ratio of the mesopore were larger than those of S-CB-mat, as shown in Table 3. These results indicate that MS-CB-mat was not sufficiently activated by steam. As steam activation of CB powder itself led to only a slight increase in the BET surface area from 63 to 96 m^2 g^{-1} (Table 3), it is suggested that the CB resisted the steam activation. Therefore, it can be considered that the CB fine powders, widely distributed on the surface (and inside) of the electrospun HKL fibers (Figure S5), hampered the efficient activation of the fibers in MS-CB-mat while contributing to the reduction of the surface resistance of the mat.

Finally, an EDLC was assembled with E-MS-CB-mat and tHKL separator. The resultant EDLC with E-MS-CB-mat exhibited better capacitance, energy density, and power density than those of the EDLC with E-S-CB-mat (Table 1). Particularly, its power density was two times higher than that of the EDLC with E-S-CB-mat. Moreover, its energy density was higher than that of the EDLC with E-S-CB-powder. The enhanced performance might be attributed to the mesopore development in E-MS-CB-mat in addition to its sufficiently low surface roughness and resistance. This mesopore development was clearly observed in the N$_2$ adsorption–desorption isotherms of Figure 4, where the area of hysteresis at the P/P_0 range of 0.5–1.0 revealed the mesopore volume. The area for MS-CB-mat was distinctly larger than that for S-CB-mat,
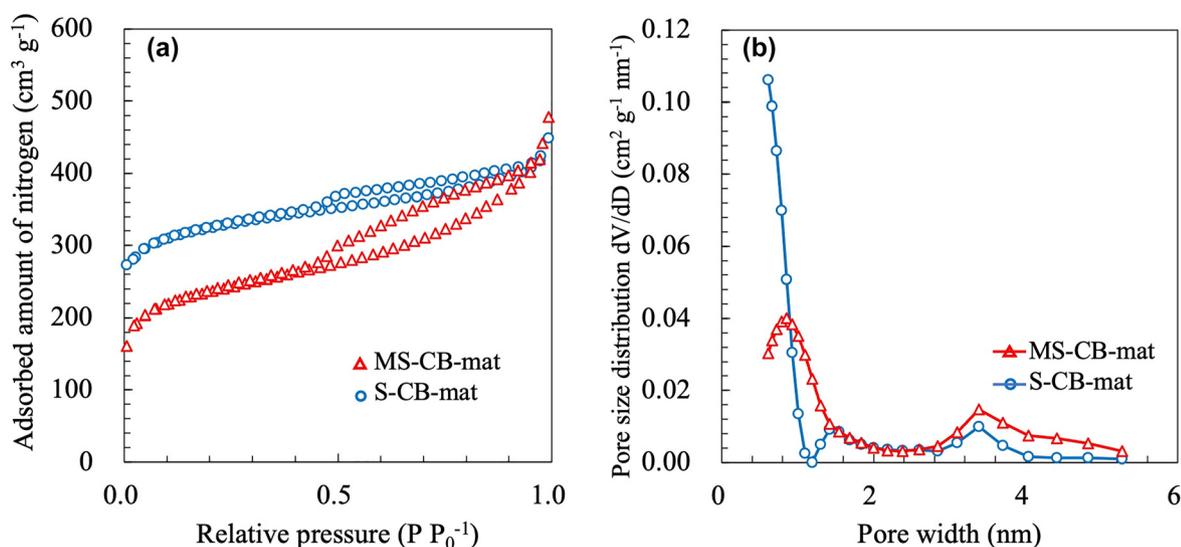
Figure 4: BET analysis of S-CB-mat and MS-CB-mat; (a) N$_2$ adsorption–desorption isotherms and the calculated (b) pore-size distribution curves.

indicating that the generated micropores were developed into mesopores, despite the steam activation did not sufficiently improve the surface area due to the presence of CB fine powders distributed in the HKL fibers (Figure S5).

A stability test of the EDLCs for a long time was attempted as shown in Figure S6. However, the performance of EDLCs with HKL-based separator and even a commercial cellulosic separator reduced to 60–80% at 100 times. Therefore, the insufficient stability observed might be caused by the experimental condition rather than the intrinsic performances of the EDLCs. Precisely, all EDLCs were assembled in a glove box, but it was not completely closed; thereby, causing the contamination of a small amount of water into the measurement cell. Such water in the assembled EDLCs might have caused the early degradation of performances in the long-time tests.

4 Conclusions

This study demonstrated the facile preparation of a separator and two types of electrodes from an electrospun HKL fiber mat and their combinational application for EDLCs. The EDLC assembled with a mat-type electrode (MS-CB-mat) and tHKL separator possessed high energy and power densities, compared to the previously reported EDLCs (Figure S7, where the energy and power densities of lignin-based EDLCs are summarized). Although a powder-type electrode (E-S-CB-powder) required arduous preparation by grinding ACFs and re-forming into a sheet by a casting method, its EDLC exhibited excellent electrochemical performance; especially, high power density, which was attributed to the smooth surface of the powder-type electrode and the resultant good contact with the separator. Thus, the assembly of this HKL-based separator and electrodes together with an EmimBF$_4$ electrolyte results in a promising EDLC.

References

Chakrabarti, B.K. and Low, C.T.J. (2021). Practical aspects of electrophoretic deposition to produce commercially viable supercapacitor energy storage electrodes. RSC Adv. 11: 20641–20650.

Du, B., Zhu, H., Chai, L., Cheng, J., Wang, X., Chen, X., Zhou, J., and Sun, R.C. (2021). Effect of lignin structure in different biomass resources on the performance of lignin-based carbon nanofibers as supercapacitor electrode. Ind. Crop. Prod. 170: 113745.

Fthenakis, V.M. and Nikolakakis, T. (2012). Storage options for photovoltaics. In: Sayich, A. (Ed.), *Comprehensive renewable energy*. Elsevier, Oxford, UK, pp. 199–212.

Funabashi, T. (2016). *Integration of distributed energy resources in power systems: implementation, operation and control*, 1st ed. Academic Press, Massachusetts, pp. 1–14.

García-Mateos, F.J., Ruiz-Rosas, R., Rosas, J.M., Morallón, E., Cazorla-Amorós, D., Rodríguez-Mirasol, J., and Cordero, T. (2020). Activation of electrospun lignin-based carbon fibers and their performance as self-standing supercapacitor electrodes. Separ. Purif. Technol. 241: 116724.

Hamsan, M., Aziz, S.B., Kadir, M., Brza, M., and Karim, W.O. (2020). The study of EDLC device fabricated from plasticized magnesium ion conducting chitosan based polymer electrolyte. Polym. Test. 90: 106717.

He, T., Jia, R., Lang, X., Wu, X., and Wang, Y. (2017). Preparation and electrochemical performance of PVDF ultrafine porous fiber separator-cum-electrolyte for supercapacitor. J. Electrochem. Soc. 164: 379–384.

Hu, S., Zhang, S., Pan, N., and Hsieh, Y.L. (2014). High energy density supercapacitors from lignin derived submicron activated carbon fibers in aqueous electrolytes. J. Power Sources 270: 106–112.

Jiang, L., Sheng, L., and Fan, Z. (2017). Biomass-derived carbon materials with structural diversities and their applications in energy storage. Sci. China Mater. 61: 133–158.

Kasprzak, D., Stępniak, I., and Galiński, M. (2018). Electrodes and hydrogel electrolytes based on cellulose: fabrication and characterization as EDLC components. J. Solid State Electrochem. 22: 3035–3047.

Kim, T., Jung, G., Yoo, S., Suh, K.S., and Ruoff, R.S. (2013). Activated graphene-based carbons as supercapacitor electrodes with macro- and mesopores. ACS Nano 7: 6899–6905.

Koda, K., Taira, S., Kubota, A., Isozaki, T., You, X., Uraki, Y., Sugimura, K., and Nishio, Y. (2019). Development of lignin-based terpolyester film and its application to separator material for electric double-layer capacitor. J. Wood Chem. Technol. 39: 198–213.

Köse, K.Z., Pişkin, B., and Aydınol, M.K. (2018). Chemical and structural optimization of ZnCl$_2$ activated carbons via high temperature CO$_2$ treatment for EDLC applications. Int. J. Hydrogen Energy 43: 18607–18616.

Lai, C.C., Hsu, F.H., Hsu, S.Y., Deng, M.J., Lu, K.T., and Chen, J.M. (2021). 1.8 V aqueous symmetric carbon-based supercapacitors with agarose-bound activated carbons in an acidic electrolyte. Nanomaterials 11: 1731.

Li, T., Ma, R., Lin, J., Hu, Y., Zhang, P., Sun, S., and Fang, L. (2019). The synthesis and performance analysis of various biomass-based carbon materials for electric double-layer capacitors: a review. Int. J. Energy Res. 44: 2426–2454.

Lin, J., Koda, K., Kubo, S., Yamada, T., Enoki, M., and Uraki, Y. (2013). Improvement of mechanical properties of softwood lignin-based carbon fibers. J. Wood Chem. Technol. 34: 111–121.

Martin, C., Ronda, J.C., and Cadiz, V. (2006). Development of novel flame-retardant thermosets based on boron-modified phenol-formaldehyde resins. J. Polym. Sci. Polym. Chem. 44: 3503–3512.

Mei, B.A., Munteshari, O., Lau, J., Dunn, B., and Pilon, L. (2017). Physical interpretations of nyquist plots for edlc electrodes and devices. J. Phys. Chem. C 122: 194–206.

Miller, J.R. and Butler, S. (2021). Measurement of gas pressure in packaged electric double layer capacitors. J. Power Sources 509: 230366.

Najib, S. and Erdem, E. (2019). Current progress achieved in novel materials for supercapacitor electrodes: mini review. Nanoscale Adv. 1: 2817–2827.

Neimark, A.V., Lin, Y., Ravikovitch, P.I., and Thommes, M. (2009). Quenched solid density functional theory and pore size analysis of micro-mesoporous carbons. Carbon 47: 1617–1628.

Nguyen, H.V.T., Kim, J., and Lee, K.K. (2021). High-voltage and intrinsically safe supercapacitors based on a trimethyl phosphate electrolyte. J. Mat. Chem. A 9: 20725–20736.

Nguyen, N.T., Le, P., and Phung, V.B.T. (2020). Biomass-derived activated carbon electrode coupled with a redox additive electrolyte for electrical double-layer capacitors. J. Nanoparticle Res. 22: 371.

Nguyen, T.Q. and Breitkopf, C. (2018). Determination of diffusion coefficients using impedance spectroscopy data. J. Electrochem. Soc. 165: 826–831.

Pai, J.Y., Hsieh, C.T., Lee, C.H., Wang, J.A., Ku, H.Y., Huang, C.L., Hardwick, L.J., and Hu, C.C. (2021). Engineering of electrospun polyimide separators for electrical double-layer capacitors and lithium-ion cells. J. Power Sources 482: 229054.

Pakkang, N., Kumar, M., Taira, S., Koda, K., Shigetomi, K., and Uraki, Y. (2020). Preparation of kraft lignin-based activated carbon fiber electrodes for electric double layer capacitors using an ionic liquid electrolyte. Holzforschung 74: 577–588.

Park, J.H., Rana, H.H., Lee, J.Y., and Park, H.S. (2019). Renewable flexible supercapacitors based on all-lignin-based hydrogel electrolytes and nanofiber electrodes. J. Mater. Chem. 7: 16962–16968.

Saha, D., Li, Y., Bi, Z., Chen, J., Keum, J.K., Hensley, D.K., Grappe, H.A., Meyer, H.M., Dai, S., Paranthaman, M.P., et al. (2014). Studies on supercapacitor electrode material from activated lignin-derived mesoporous carbon. Langmuir 30: 900–910.

Suzanowicz, A.M., Lee, Y., Schultz, A., Marques, O.J.J., Lin, H., Segre, C.U., and Mandal, B.K. (2022). Synthesis and electrochemical properties of lignin-derived high surface area carbons. Surfaces 5: 265–279.

Taer, E., Apriwandi, A., Agustino, A., Dewi, M.R., and Taslim, R. (2021). Porous hollow biomass-based carbon nanofiber/nanosheet for high-performance supercapacitor. Int. J. Energy Res. 46: 1467–1480.

Taira, S., Kurihara, M., Koda, K., Sugimura, K., Nishio, Y., and Uraki, Y. (2019). TEMPO-oxidized cellulose nanofiber-reinforced lignin based polyester

films as a separator for electric double-layer capacitor. Cellulose 26: 569–580.

Takeuchi, K., Fujishige, M., Ishida, N., Kunieda, Y., Kato, Y., Tanaka, Y., Ochi, T., Shirotori, H., Uzuhashi, Y., Ito, S., et al. (2018). High porous bio-nanocarbons prepared by carbonization and NaOH activation of polysaccharides for electrode material of EDLC. J. Phys. Chem. Solid. 118: 137–143.

Uddin, M.J., Alaboina, P.K., Zhang, L., and Cho, S.J. (2017). A low-cost, environment-friendly lignin-polyvinyl alcohol nanofiber separator using a water-based method for safer and faster lithium-ion batteries. Mater. Sci. Eng. B 223: 84–90.

Wang, X., Zhou, J., and Tang, W. (2021). Emerging polymer electrodes for aqueous energy storage. Mater. Horiz. 8: 2373–2386.

Wu, H., Liu, C., Jiang, Z., Yang, Z., Mao, X., Wei, L., and Sun, R. (2021). Electrospun flexible lignin/polyacrylonitrile-based carbon nanofiber and its application in electrode materials for supercapacitors. Textil. Res. J. 92: 456–466.

Xian-Zhong, S., Xiong, Z., Bo, H., and Yan-Wei, M. (2014). Effects of separator on the electrochemical performance of electrical double-layer capacitor and hybrid battery-supercapacitor. Acta Phys. Sin. 30: 485–491.

Yan, R., Antonietti, M., and Oschatz, M. (2018). Toward the experimental understanding of the energy storage mechanism and ion dynamics in ionic liquid based supercapacitors. Adv. Energy Mater. 8: 1800026.

You, X., Koda, K., Yamada, T., and Uraki, Y. (2015). Preparation of electrode for electric double layer capacitor from electrospun lignin fibers. Holzforschung 69: 1097–1106.

You, X., Duan, J., Koda, K., Yamada, T., and Uraki, Y. (2016). Preparation of electric double layer capacitors (EDLCs) from two types of electrospun lignin fibers. Holzforschung 70: 661–671.

Zakaria, A.F., Kamaruzaman, S., and Rahman, N.A. (2021). Electrospun polyacrylonitrile/lignin/poly(ethylene glycol)-based porous activated carbon nanofiber for removal of nickel(ii) ion from aqueous solution. Polymers 13: 3590.

Zhao, M., Wang, J., Chong, C., Yu, X., Wang, L., and Shi, Z. (2015). An electrospun lignin/polyacrylonitrile nonwoven composite separator with high porosity and thermal stability for lithium-ion batteries. RSC Adv. 5: 101115–101120.

Zhu, M., Liu, H., Cao, Q., Zheng, H., Xu, D., Guo, H., Wang, S., Li, Y., and Zhou, J. (2020). Electrospun lignin-based carbon nanofibers as supercapacitor electrodes. ACS Sustain. Chem. Eng. 8: 12831–12841.